Releasing a Bound Molecular Spring with Light: A Visible Light-Triggered Photosalient Effect Tied to Polymorphism

Keegan McGehee[a,b], Dennis Kwaria[b], Koichiro Saito[b], Hiroyuki Minamikawa[c], Yasuo Norikane[b,a]

a) *Graduate School of Pure and Applied Science, University of Tsukuba, Tsukuba, Ibaraki 305-8571, Japan.*
b) *Research Institute for Advanced Electronics and Photonics, National Institute of Advanced Industrial Science and Technology (AIST), Tsukuba, Ibaraki 305-8565, Japan*
c) *Interdisciplinary Research Center for Catalytic Chemistry, National Institute of Advanced Industrial Science and Technology (AIST), Tsukuba, Ibaraki 305-8565, Japan*

Contents

Materials

1,1,2,2-tetrachlorethane was purchased from Dojindo Chemicals (Japan). Azobenzene, 1,3-dibromo-5,5-dimethylhydantoin, tetrakis(triphenylphosphine)palladium(0) were purchased from TCI (Japan). Potassium persulfate was purchased from Kishida Chemical (Japan). All reagents and solvents were used as received without further purification.

Instrumentation

For this study the following instruments were used; SII Nanotechnology DSC6220, JASCO V780, Perkin Elmer Raman Station 400F, FLIR i3 IR camera, Olympus BX51, Olympus Bx53, Newport 1917-R optical power meter with an 818-ST-UV photodetector, Rigaku xtaLab Mini, Rigaku RAXIS-IV. Light sources used were Olympus RFL-T Hg lamps with appropriate filters or LEDs from CCS. Models of LED used were as follows; HVL-24UV365-4WNRBTNJ (365 nm), HLV2-22BL-3W (465 nm), HVL2-22GR-3W (520 nm), and HVL2-22RD-3W (645 nm). Relevant additional details and operating conditions are given in the experimental methods.

Experimental Methods

Synthesis of 4Br-Azo

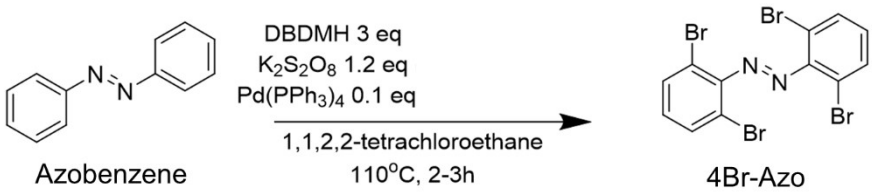

The compound 4Br-Azo was synthesized according to a previously reported procedure[1], but with the solvent changed to 1,1,2,2-tetrachlorethane (TCE) to allow reaction at ambient pressure. Typically, about 3.5 mmol (637.77 mg) azobenzene, 10.5 mmol (3.0 eq., 3.00 g) 1,3-dibromo-5,5-dimethylhydantoin, and 0.35 mmol tetrakis(triphenylphosphine)palladium(0) (0.1 eq., 404.46 mg) were placed in a 50 mL round bottom flask and dissolved in 10 mL TCE. Then 4.2 mmol (1.2 eq., 1.14 g) potassium persulfate was added to the reaction mixture before heating it to ~110 °C. The mixture was heated with stirring for about 3h to complete the reaction. Following removal of the solvent by rotary evaporation, the crude product was recovered as a red-brown solid. The product was purified by column chromatography to afford a red solid as the

final product. Isolated yield of the final product was 1.74 g (3.5 mmol, quant.).

Crystallization

For crystals of α-phase about 100 mg of 4Br-Azo powder was placed in 8 mL of ethanol or hexane and the solution was heated until all solids were dissolved. The growth solution was then loosely capped. Within a week high quality α-phase crystals had formed. Single crystals of α-phase were long, red-orange needle-like structures.

High quality single crystals of β-phase 4Br-Azo were eventually obtained reliably by adding about 200 mg of 4Br-Azo powder to 9 mL of hexane and then alternating several seconds of sonication with dropwise addition of acetone until all solids were dissolved. The solution was then loosely covered with a piece of foil and left at room temperature. After sitting for about 24h, β-phase crystals had formed at the bottom of the flask. Single crystals of β-phase were generally thin, plate-like in shape, and dark red in color. Crystallization procedures for both phases were tested in dark and ambient light conditions, with no apparent change in the results.

To fully characterize the solid-state properties of 4Br-Azo the *cis* isomer was also crystalized. This was done by taking advantage of the fact that the increased polarity of the *cis* isomer reduces the already fairly low solubility of *trans* 4Br-Azo in hexane to nearly zero. About 24 mg of 4Br-Azo was dissolved in 5 mL of hexane and sonicated. This solution was irradiated with a red (λ_{max} = 645 nm) LED in an otherwise dark environment for 1-2h to precipitate *cis* 4Br-Azo. Crystals of the *cis* isomer were a light orange color and had a small needle like shape.

Microscope Observations

Two different microscopes were used for photosalient observations. An Olympus BX51 and an Olympus BX53. Both are equipped with a RFL-T Hg lamp also from Olympus with appropriate filters. The power of the filtered light output in each setup was measured using a Newport 1917-R optical power meter with an 818-ST-UV photodetector. The irradiated area was then estimated by measuring the size of an area undergoing photoinduced crystal-to-liquid phase transition of a 4,4'-dioctyloxy-3-methyl azobenzene[2] thin film.

Intensity Dependence Experiment

Sample crystals were cut to give pieces with at least one dimension around 1 mm or more. We also note that the morphology of the crystals only makes irradiation incident to the [001] crystal face feasible. So, all experiments were performed with this configuration. The light source used was a Hg lamp which was filtered to control irradiation wavelength and intensity. Peak wavelengths of the emission bands used were 435 nm (violet), 480 nm (blue), and 546 nm

(green). For each light condition the photosalient response time was measured for 3 different crystals, giving a total crystal sample size of 36 crystals. In the main text Fig. 2c. presents the averaged values of those measurements. Full details on the irradiation conditions used are shown in Table S2.

DSC Measurements

Samples of 4Br-Azo (~0.5-4 mg) were placed in a sealed Al pan and measured relative to an empty Al reference pan. The temperature range measured was 50-130 °C for experiments conducted without melting and 30-150 °C for experiments where the sample was melted. Samples were held at the final temperature of a heating/cooling ramp for 5 min before starting the next ramp. At least two heat-cool cycles were conducted for each sample. Heating and cooling rates were varied between 5K, 15K, or 25K min^{-1} to test different thermal responses.

Raman Spectroscopy

Raman spectra were measured using a Perkin Elmer RamanStation 400F with a 785 nm laser. The laser was set to 5% power (~12.5 mW) for typical measurements and data was collected as the accumulation of 50 1s collection periods. Background was removed from measured spectra using the Spectrum™ software from Perkin Elmer.

XRD Measurements

Single crystal XRD was carried out using a Rigaku XtaLAB Mini diffractometer using monochromatic MoKα radiation (λ = 0.71075 Å). Crystals were cooled to 170K for diffraction measurements. Collected diffraction data was used to solve all crystal structures by direct methods followed by least-squares structure refinement with SHELXL97[3] . Hydrogens were refined using the riding hydrogen model. Full data such as number of reflections, data reduction, and all cell parameters for each experiment can be found in Table S1. The largest exposed face of the β-phase, which was observed and irradiated for all experiments, was determined to be [001] using CrysAlisPro.

Powder XRD experiments were performed on a Rigaku RAXIS-IV diffractometer using monochromatic CuKα radiation (λ = 1.542 Å). Samples were placed in a Mettler FP82HT hot stage sample holder. Typically, samples were powdered 4Br-Azo crystals sandwiched between two layers of polyimide film (film thickness = 12.5 μm). Detector plates (Fuji-Film Image plate) with dimensions of 30 cm x 30 cm were used as a flat camera film. A sample-to-camera length of 100.0 mm or 150.0 mm was used.

Light Induced Phase Transition Experiment

Approximately 1 mg of β-phase 4Br-Azo powder loosely pressed in a thin layer was sealed between two pieces of colorless polyimide film (thickness ~ 12.5 μm). Light from a focused 465 nm LED (I ~ 500 mW cm^{-2}) was shone on the sample at normal incidence. After a 5 min period of irradiation the LED was turned off and the Raman spectrum of the sample was measured. This process was repeated until two identical Raman spectra were measured. Presented Raman spectra have the background polyimide signal subtracted. The PXRD pattern of the final sample was measured in the irradiated and unirradiated areas. During the irradiation period for the sample, the surface temperature of the powder was measured using a FLIR i3 IR camera. Measurement showed a maximum temperature of 45 °C in the irradiated area. The unirradiated area did not rise above room temperature.

Measurements of Sample Dimensions

The thickness of crystals used for photosalient observations and spectroscopy measurements were measured using a Keyence VK-X100 laser confocal microscope with a laser wavelength of 658 nm.

Crystallography Details

Table S1. Crystallographic details of the trans isomer polymorphs and the cis isomer

	trans *α-phase*	trans *α-phase*	cis *4Br-Azo*
Chemical Formula	$C_{12}N_2Br_4H_6$	$C_{12}N_2Br_4H_6$	$C_{12}N_2Br_4H_6$
Space group	C 2/c	P 2_1/c	P 2_1/c
Crystal System	Monoclinic	Monoclinic	Monoclinic
Temperature (K)	170	170	170
Cell Lengths (Å)	**a** = 15.64(4) **b** = 12.14(3) **c** = 8.31(2)	**a** = 23.306(11) **b** = 8.580(4) **c** = 14.137(7)	**a** = 11.13(2) **b** = 7.520(13) **c** = 16.82(3)
Cell angles (°)	β = 112.61 α = γ = 90.00	β =102.08 α = γ = 90.00	β =109.223 α = γ = 90.00
Cell volume ($Å^3$)	1457.7	2764.3	1329.3
Z, Z’	4, 1	8, 2	4, 1
R[a]	0.0638	0.0411	0.1144
wR_2[b]	0.1964	0.0836	0.2767
S[c]	1.139	1.015	1.120
ρ_{calc} (g cm^{-3})	2.270	2.370	2.488
μ (mm^{-1})	11.031	11.528	12.094
Reflect. Collected	1660	9693	3124
Reflect. Observed (I > 3σ(I))	1143	6579	1837

[a] $R_1 = \sum(|Fo| - |Fc|)/\sum|Fo|$. [b] $wR_2 = [\sum w(Fo^2 - Fc^2)^2 / \sum w(Fo^2)^2]^{1/2}$. [c] $S = [\sum w(|Fo| - |Fc|)^2 / (No - Np)]^{1/2}$

Additional Details on Intensity Dependence Observations

The following table details the average response times and associated standard deviations shown graphically in Fig. 2c. It also contains observations on the irradiation conditions that were tested but did not show a photosalient effect on the sampled crystal set. Under the current recording conditions resolving the response time below 1 s frames was not feasible, so all times were recorded to the nearest second. Reported response data is the result of at least three measurements at each irradiation condition. An entry of "no visible response" or "only cracking" is the conclusion of observing one minute of irradiation time.

Table S2. Details of the response time versus intensity measurements presented in Fig. 2c.

Entry	λ_{peak} (nm)	Intensity (mw cm^{-2})	Response time (s)
1	435	300	only cracking
2	435	300	only cracking
3	435	300	only cracking
4	435	1200	4
5	435	1200	7
6	435	1200	10
7	435	3500	1
8	435	3500	5
9	435	3500	3
10	480	70	no visible response
11	480	70	no visible response
12	480	70	no visible response
13	480	200	only cracking
14	480	200	only cracking
15	480	200	only cracking
16	480	700	9
17	480	700	25
18	480	700	18
19	480	1000	4
20	480	1000	11
21	480	1000	3
22	480	3900	4
23	480	3900	3
24	480	3900	2
25	546	200	only cracking
26	546	200	only cracking
27	546	200	only cracking
28	546	600	6
29	546	600	12
30	546	600	20
31	546	2500	7
32	546	2500	3

33	546	2500	2
34	546	3100	3
35	546	3100	2
36	546	3100	6

Two Olympus microscopes (Models BX51 and BX53) outfitted with RFL-T Hg lamps were used for observing photosalient behaviors in this study. Both are equipped with wavelength filters to select the color of light supplied to the sample and one also has natural density (ND) filters for tuning the supplied power. Pairs of wavelength filter names and characteristic emission peaks allowed through (F,λ_{peak}) are as follows; (WBV, 404/435 nm), (NBV, 435 nm), (NB, 480 nm), and (NG,546 nm) The ND filters used are labeled in the following table as ND1 and ND2, which have fractional transmittances of 25% and 6% respectively. The tables below list the measured intensities rounded to the nearest 100 mW/cm^2 for the available filter configurations on each microscope. On the BX53 microscope only the NB filter was used without ND filters as the other wavelengths were strong enough to damage 4Br-Azo. The WBV with ND1 condition is also excluded as the response time with that condition was too fast to be properly evaluated along with the others.

BX53

Wavelength Filter	ND1 + ND2	ND2	ND1	No ND Filter
WBV	300	1200	N/A	N/A
NB	70	200	1000	3900
NG	200	600	2600	N/A

BX51

Wavelength Filter	Intensity (mW/cm^2)
NBV	3500
NB	700
NG	3100

Solid State Absorption

The solid-state absorption properties of each polymorph were measured using an Olympus BX53 customized for microscope spectroscopy. A Xe lamp was used as a white light source and the intensity of the light passed through the microscope lens was measured with an Ocean Optics Flame spectrometer. A Thor Labs LMM-15X-UVV lens was used for these measurements. The α-phase sample was prepared by melting a few mg of 4Br-Azo powder on a glass cover slip, then placing a second cover slip on top before cooling to obtain a thin film with a measured thickness of ~20 μm. The β-phase sample was a thin crystal with a measured thickness of 10 μm placed on the same type of glass cover slips. To collect the presented data, first the incident light from the Xe lamp was measured on an empty glass area. Then the intensity of the light transmitted through the 4Br-Azo sample was measured. These values were then used to calculate percent transmittance followed by absorbance. All measurements are from 25000 μs of collection time.

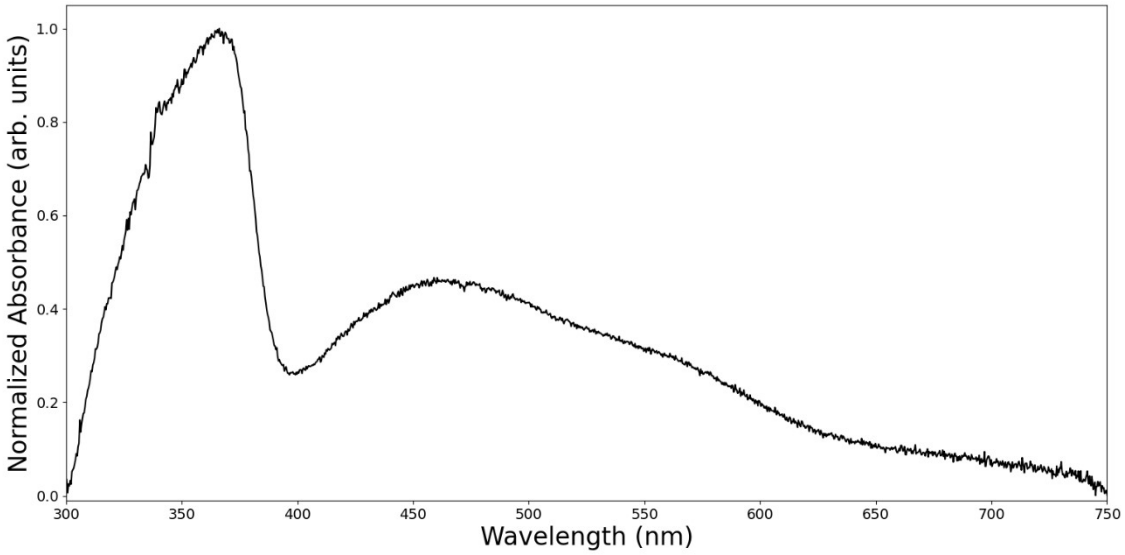

Figure S1. Absorbance spectrum from 300-750 nm of β-phase 4Br-Azo. Sample was a 10 μm thick single crystal.

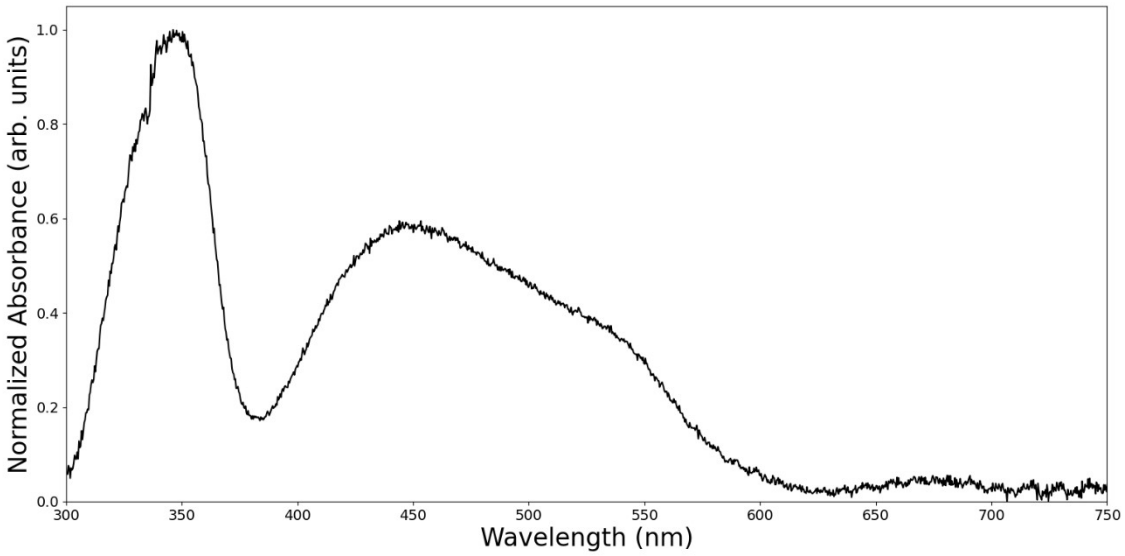

Figure S2. Absorbance spectrum from 300-750 nm of α-phase 4Br-Azo. Sample was a thin film prepared from melted 4Br-Azo placed between two glass cover slips. Film thickness was measured as ~20 μm.

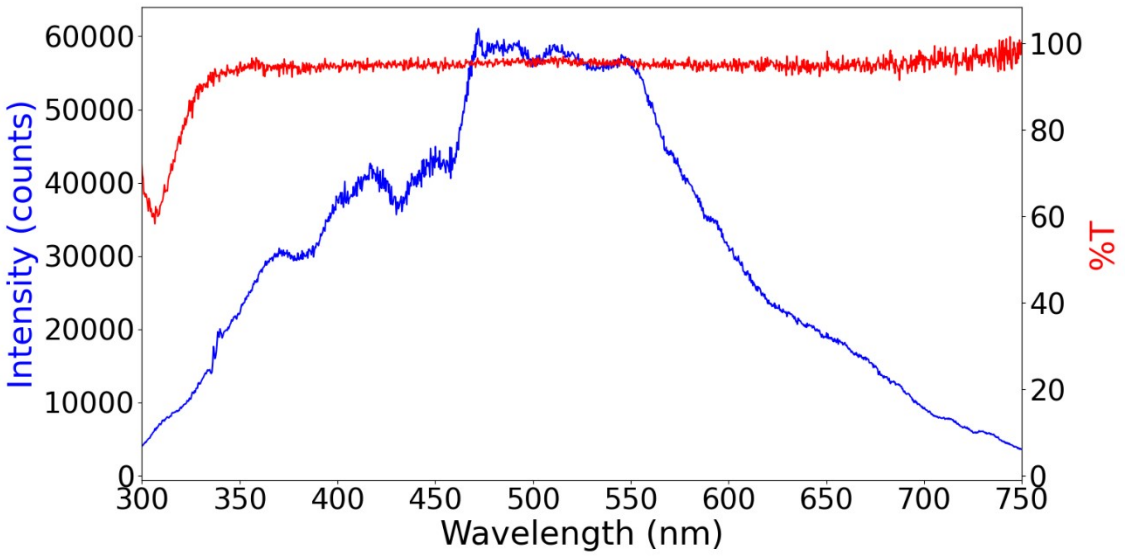

Figure S3. Emission spectrum of the Xe lamp used as a light source (blue line) and the percent transmittance of the glass substrate used for measurement (red line).

DSC Data

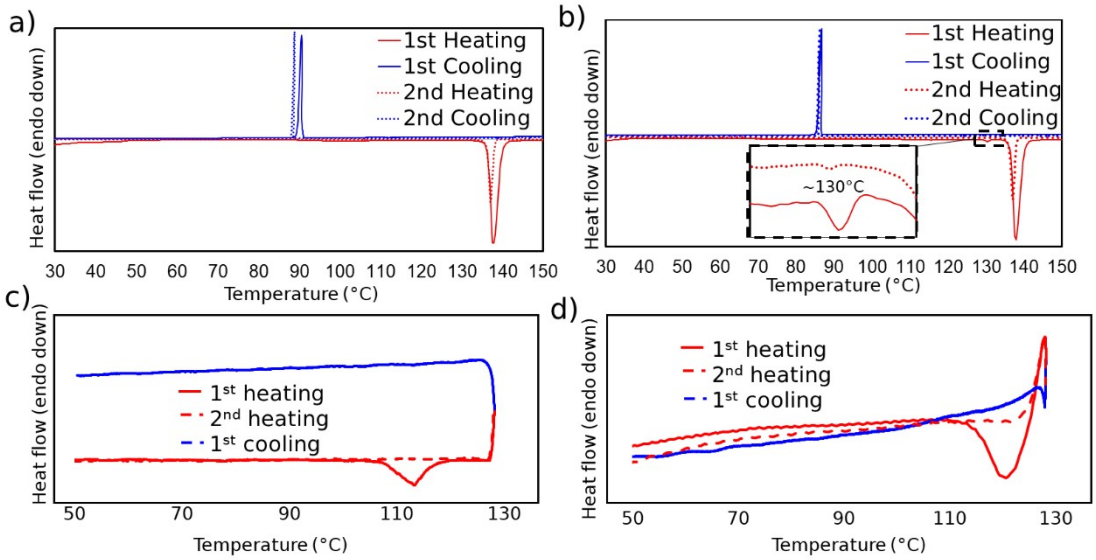

Figure S4. DSC data for two heating/cooling cycles of the α-phase (a) and β-phase (b) crystals. Here heating rates are 15°C/min. No melt DSC cycles of β-phase powder heated at 5 °C/min (c) and 25 °C/min (d). All cooling rates are 5 °C/min.

Solution UV-Vis Spectroscopy

A concentrated solution of 4Br-Azo in chloroform was irradiated with a green (520 nm nm) LED overnight to afford a solution containing a significant amount of *trans* and *cis* isomers. The solvent was removed using a rotary evaporator and then the mixed isomer sample was separated using column chromatography to afford pure samples of the two isomers. Aliquots of both isomers dissolved in chloroform with a concentration of 5.0 x 10^{-5} M were prepared to measure the pure isomer spectra presented in Figure S5 It was found that in the solution state the photoswitchability of 4Br-Azo is relatively low. The 365 nm and 520 nm PSSs presented in Figure S5 do appear to show reasonable conversion to the *cis* isomer but require a relatively long time to reach. On the other hand, switching from a *cis* rich solution could not be accomplished quickly enough to be certain that thermal isomerization was not as much or more of a factor. Solution state absorption was measured with a JASCO V780 spectrometer.

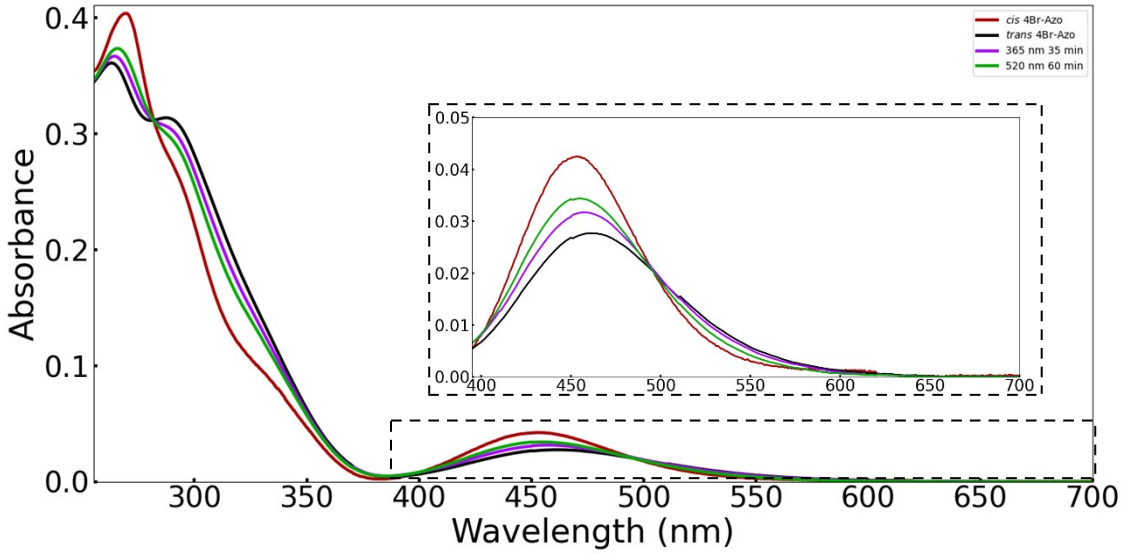

Figure S5. Pure isomer, 365 nm PSS, and 520 nm PSS UV-Vis absorption spectra of 4Br-Azo in chloroform (5.0 x 10^{-5} M).

Additional Characterization of *cis* 4Br-Azo

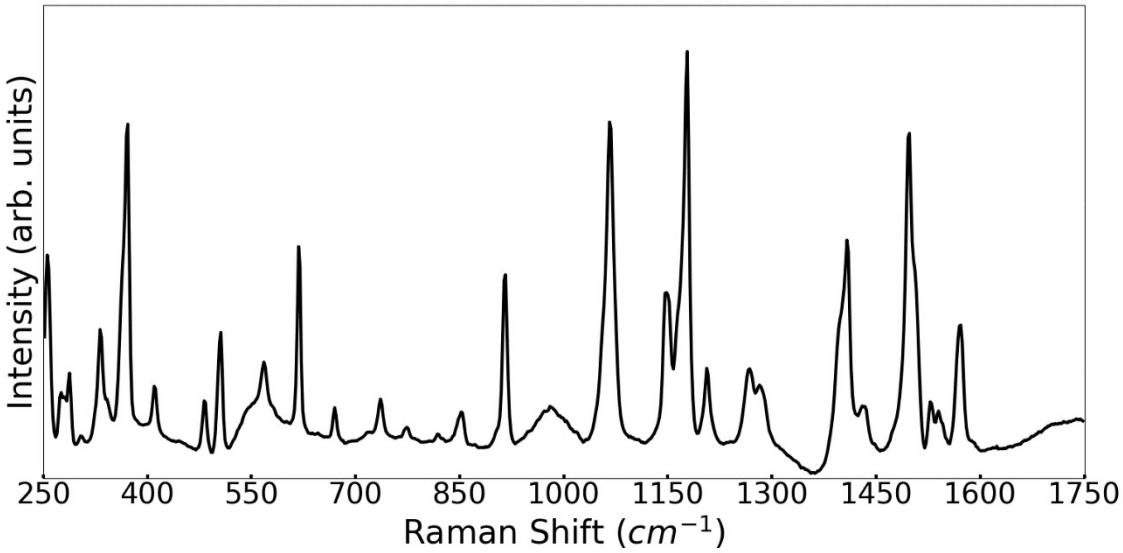

Figure S6 Raman spectrum of powdered *cis* 4Br-Azo.

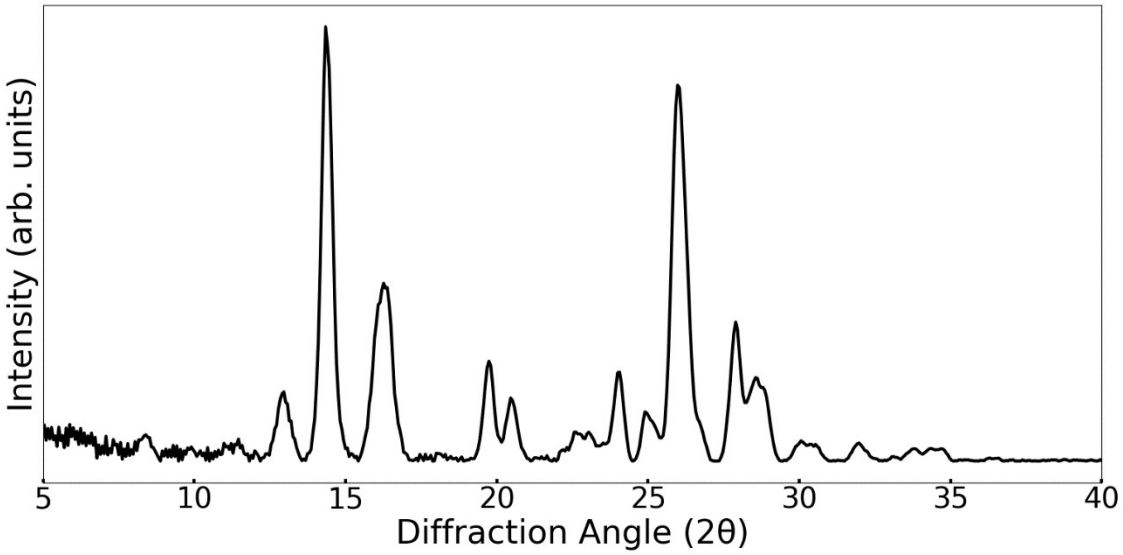

Figure S7. Powder XRD pattern of *cis* 4Br-Azo

Computational Methods

DFT Calculations

All single molecule DFT calculations were carried out using Gaussian 16[4]. The hybrid functional B3LYP was selected for its generally accepted reliability for geometry optimization and ground state single point energy calculations of small organic molecules. To account for intramolecular Van der Waals forces, which have been found to impact the geometry and energy of azobenzene derivatives significantly[5], Grimme's D3[6] (GD3) empirical dispersion correction

was added. Geometries were optimized with 6-311G(d). Optimized gas phase geometries were calculated with no restrictions. Frequency calculations were done to obtain zero-point energy corrections and confirm the stationary states had no negative values in their Hessian matrix. Final reported energies are from single point calculations using cc-pvtz. Calculations on the crystal phase conformations were done by extracting the molecular coordinates from the CIF files created by refinement of the SCXRD data. The C-H bond distances in these geometries were set to standard reference values of aryl C-H bonds measured by neutron diffraction[7]. For the β_{high} conformer the presented energy in Table 1 is a weighted average of single point energies calculated with only one of the disordered parts modeled at a time. Vertical excitation energies of the conformers were also calculated using TDDFT. For these calculations the CAM-B3LYP/6-311G(2d,p) level of theory was used.

Lattice Energy Calculations

Within Crystal Explorer21[8] (CE) energy calculations are based on easily calculable "monomer" wavefunctions at the B3LYP/6-31G(d,p) level for each symmetry unique molecule in a crystal. From there it is simple to calculate the interaction energy between two molecules in the crystal using the following equation.

$$E_{tot} = E_{ele} + E_{pol} + E_{dis} + E_{rep}$$

Where E_{tot}, E_{ele}, E_{pol}, E_{dis}, and E_{rep} are total, electrostatic, polarization, Grimme's D2 dispersion, and exchange-repulsion interaction energies, respectively. Each term additionally has a coefficient, *k*, which has been calibrated by the CE authors using a large model dataset[9,10]. The CE method for lattice energy (LE) calculations involves summing the E_{tot} values across a cluster of molecules and dividing by two to avoid double counting. In this work the recommended method of performing this calculation for progressively larger clusters of molecules until a difference of less than 0.5 kJ/mol is found between steps was followed[10]. Importantly, one should note that this process is done by selecting one symmetry unique molecule and producing a list of all pairwise interaction energies between it and other molecules in the selected cluster. Thus, when Z' > 1, like in 4Br-Azo β-phase, it is necessary to do the described LE sum for each unique molecular conformation and average the results to get the LE for the whole crystal. Additionally, to account for the disorder of the β_{high} conformer this LE calculation was first done for the case where one disordered part was considered at full occupancy. Then the calculation was repeated with the other disordered sites considered at full occupancy and the weighted average of the two LE values was taken following the reported occupancy of each part (Fig. 4c). This final weighted average value has been presented in this work.

TDDFT

Vertical excitation energies for both the fully optimized and crystal phase conformers were calculated at the CAM-B3LYP/6-311G(2d,p) level. For the fully optimized structure these calculation parameters along with a polarizable continuum model for solvation showed good agreement with the measured solution state spectrum in chloroform. With the measured and calculated values of λ_{peak} for the n-π^* band being 461 nm and 469 nm respectively for the *trans* isomer. Thus, it was considered that the trends of interest for the other *trans* conformations would also be observable with this functional and basis set. Detailed numbers are shown in Table S3, but Figure S7 is included as a visual summary. Effectively these modeled UV-Vis spectra show that we expect more broad bands in the β-phase due to the contribution of multiple molecular conformations compared the α-phase with its single conformation. Though this type of single molecule calculation does not reflect the electron density smearing that gives the much greater peak distortion that we actually observe in a solid-state measurement, the qualitative differences particularly in the visible absorption region are well rationalized from the single molecule calculations.

Table S3. Details on the first five calculated singlet excitations of the fully optimized geometries of *trans* and *cis* isomers as well as the crystal state conformations of *trans* 4Br-Azo. Percentages next to the crystal conformers correspond to their weighting in Figure S5. All values are calculated at the CAM-B3LYP//6-311G(2d,p) level of theory. *Values contain an additional PCM solvent model for chloroform.

CONFORMATION (WT%)	**$S_0 \rightarrow S_1$ WAVELENGTH OSCILLATOR STRENGTH**	**$S_0 \rightarrow S_2$ WAVELENGTH OSCILLATOR STRENGTH**	**$S_0 \rightarrow S_3$ WAVELENGTH OSCILLATOR STRENGTH**	**$S_0 \rightarrow S_4$ WAVELENGTH OSCILLATOR STRENGTH**	**$S_0 \rightarrow S_5$ WAVELENGTH OSCILLATOR STRENGTH**
trans*-opt	468.99 nm	283.61 nm	280.88 nm	274.78 nm	262.98 nm
	0.0249	0.047	0.0412	0.3711	0
cis*-opt	468.64 nm	286.15 nm	285.92 nm	273.57 nm	263.69 nm
	0.0194	0.0153	0.0622	0.0099	0.2505
α (100)	453.07 nm	278.06 nm	275.28 nm	266.26 nm	257.15 nm
	0.009	0.028	0.0196	0.2305	0
β_{low} (50)	427.87 nm	270.85 nm	269.23 nm	263.94 nm	261.96 nm
	0.007	0.0233	0.0088	0.0261	0.1459
β_{high} PART 1 (27.5)	520.82 nm	305.02 nm	294.78 nm	287.74 nm	256.44 nm
	0.0164	0.1902	0.0517	0.205	0.0081
β_{high} PART 2 (22.5)	403.06 nm	267.24 nm	264.38 nm	253.44 nm	248.43 nm
	0.0047	0.0399	0.0277	0.1304	0.0101

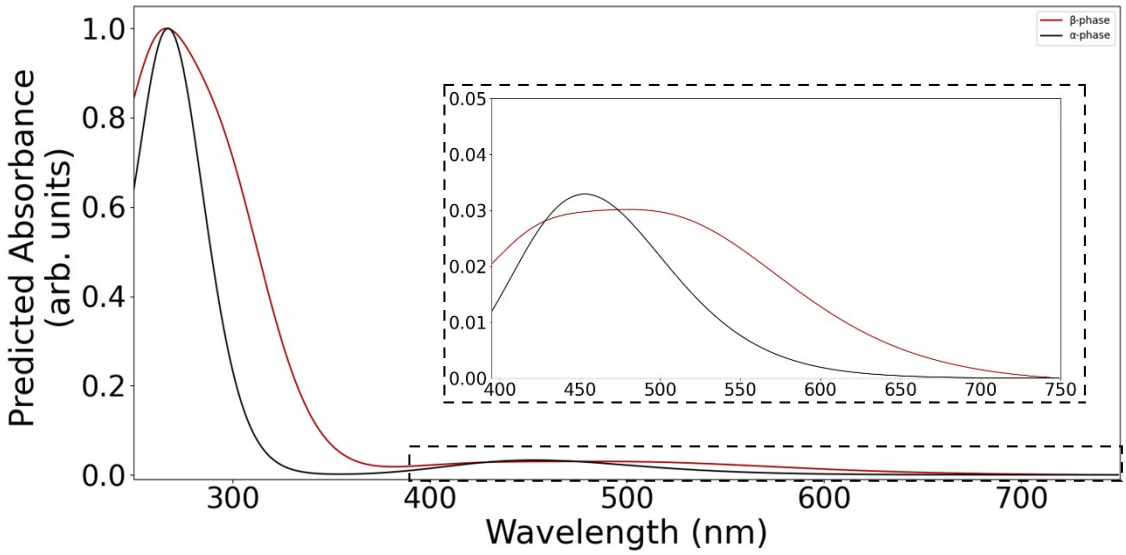

Figure S8. Visualization of the calculated vertical excitation energies of the crystal state molecular conformations found in *trans* 4Br-Azo using a summation of Gaussian band functions centered at the excitation energies shown in Table S3. Weighting coefficients for the β-phase conformers are also given in Table S2. A half-width at half height (σ) value of 0.333 eV was used.

Simulated Diffraction Patterns of Each *trans* Phase and *cis* 4Br-Azo

Simulated powder diffraction patterns are calculated based on the solved crystal structures. These visualizations are created using data from Mercury with the x-ray wavelength set to 1.542 Å to match the experimental PXRD conditions. The reflection lists used to generate these plots were used to assign characteristic peaks of the phases.

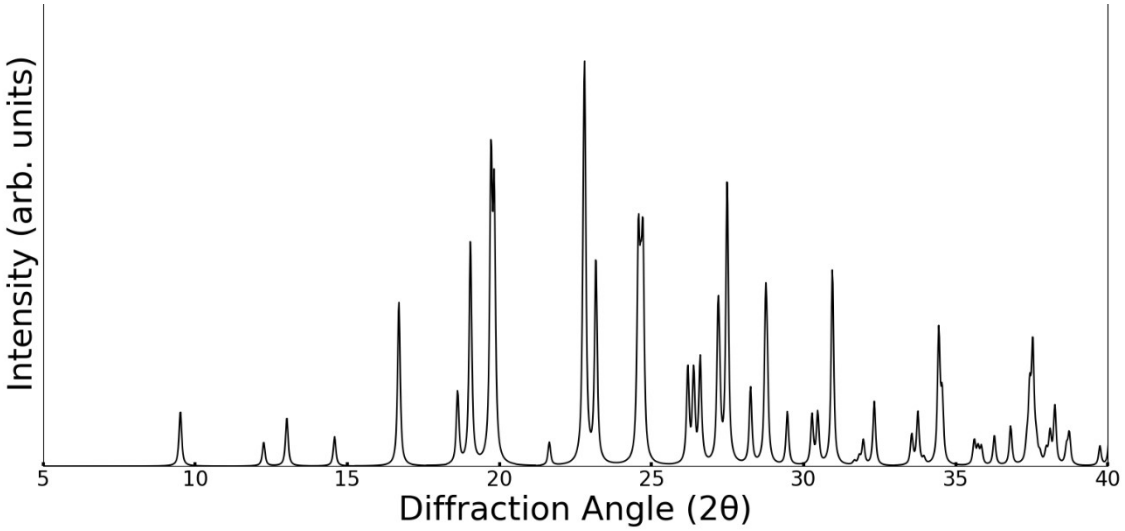

Figure S9 Predicted PXRD pattern of α-phase 4Br-Azo from λ = 1.542 Å (CuKα) x-ray.

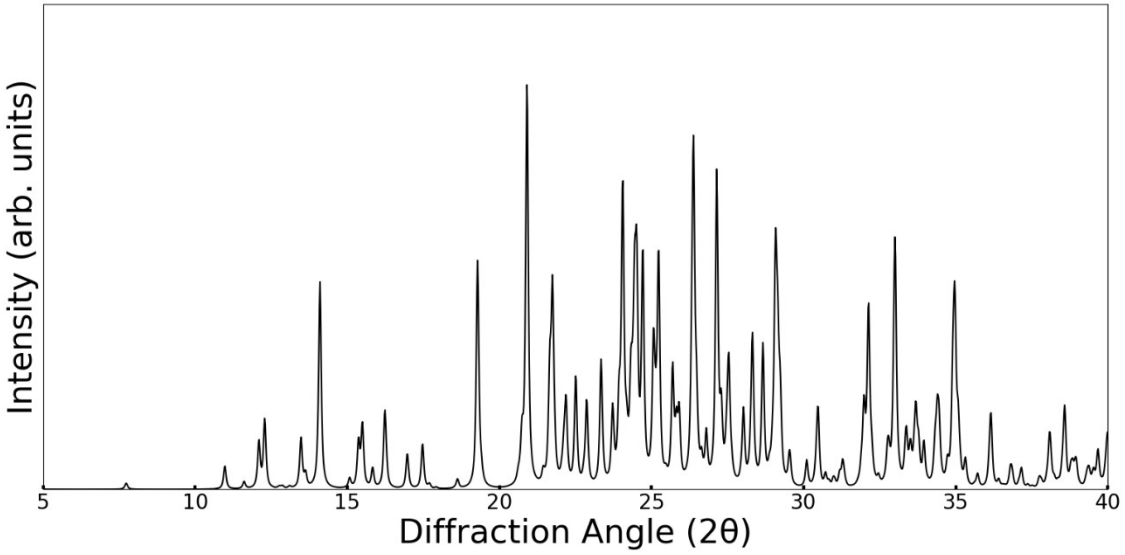

Figure S10 Predicted PXRD pattern of β-phase 4Br-Azo from λ = 1.542 Å (CuKα) x-ray.

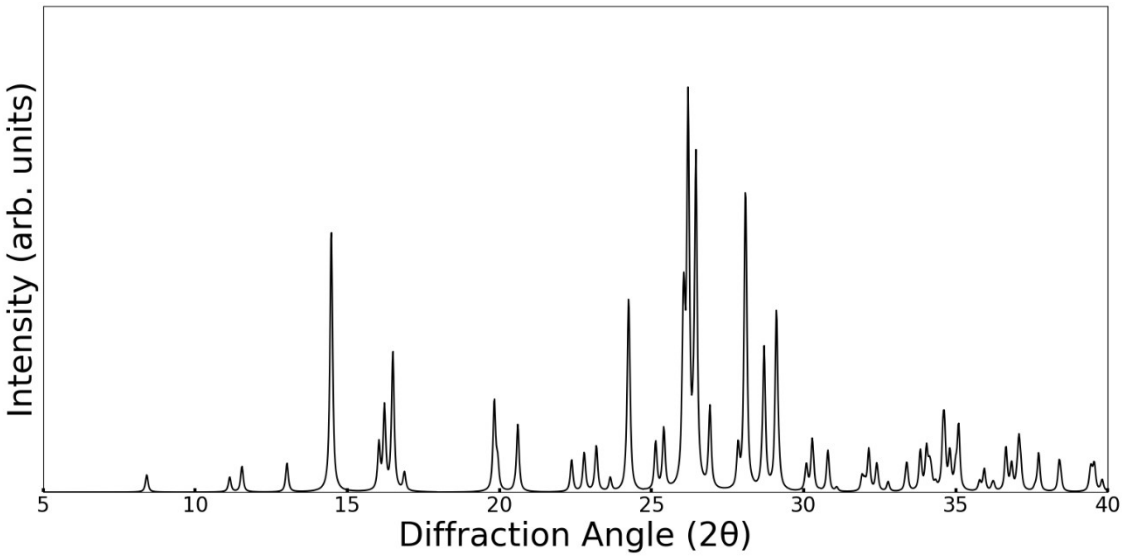

Figure S12 Predicted PXRD pattern of *cis* 4Br-Azo from λ = 1.542 Å (CuKα) x-ray.

Close Contact Interactions in α-phase and β-phase

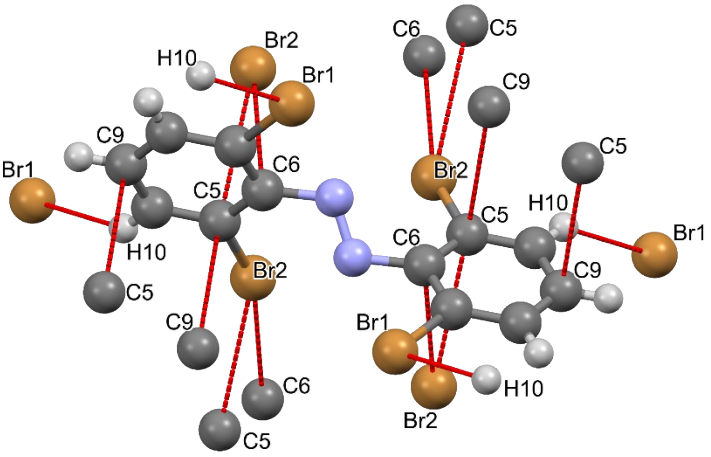

Figure S13 Expanded close contact (< sum of vdW radii - 0.01 Å) diagram of α-phase 4Br-Azo

Table S4 Close contact interactions within the α-phase crystal structure of 4Br-Azo

Atom1	Atom2	Length (Å)	Length-VdW (Å)	Symm. op. 1	Symm. op. 2
Br1	H10	3.031	-0.019	x,y,z	1/2-x,-1/2+y,1/2-z
Br2	C5	3.498	-0.052	x,y,z	x,2-y,-1/2+z
Br2	C6	3.514	-0.036	x,y,z	x,2-y,-1/2+z
C5	C9	3.34	-0.060	x,y,z	1/2-x,1.5-y,-z

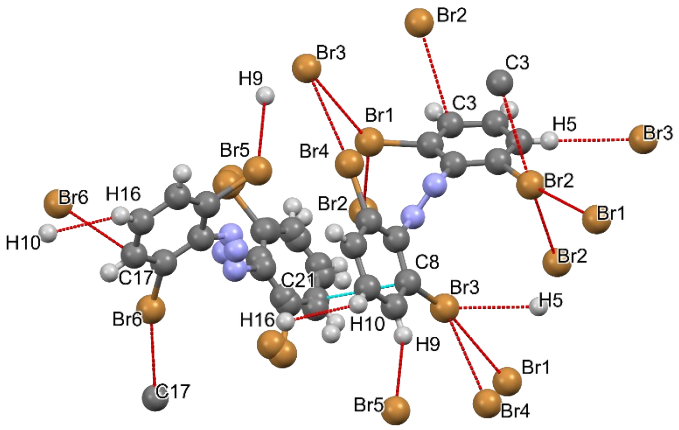

Figure S14 Expanded close contact (< sum of vdW radii - 0.01 Å) diagram of β -phase 4Br-Azo.

Table S5 Close contact interactions within the β-phase crystal structure of 4Br-Azo

Atom1	Atom2	Length (Å)	Length-VdW(Å)	Symm. op. 1	Symm. op. 2	Br···Br contact type
Br4	Br3	3.64	-0.060	x,y,z	x,-1+y,z	Type II
Br2	C3	3.524	-0.026	x,y,z	1-x,1-y,1-z	N/A
Br2	Br2	3.618	-0.082	x,y,z	1-x,2-y,1-z	Type I
Br3	H5	2.954	-0.096	x,y,z	1-x,2-y,1-z	N/A
Br2	Br1	3.446	-0.254	x,y,z	x,1.5-y,-1/2+z	Type II
C8	C21	3.358	-0.042	x,y,z	x,y,z	N/A
H9	Br5	3.011	-0.039	x,y,z	x,1+y,z	N/A
C17	Br6	3.219	-0.331	x,y,z	-x,-1/2+y,1.5-z	N/A

References

1 Q. Liu, X. Luo, S. Wei, Y. Wang, J. Zhu, Y. Liu, F. Quan, M. Zhang and C. Xia, Palladium-catalyzed direct ortho C[sbnd]X bond construction via C[sbnd]H activation of azobenzenes: Synthesis of (E)-1,2-b(2,6-dibromo(chloro)-phenyl)diazene, *Tetrahedron Lett.*, 2019, **60**, 1715–1719.

2 Y. Norikane, E. Uchida, S. Tanaka, K. Fujiwara, H. Nagai and H. Akiyama, Photoinduced phase transitions in rod-shaped azobenzene with different alkyl chain length, *J. Photopolym. Sci. Technol.*, 2016, **29**, 145–148.

3 G. M. Sheldrick, A short history of SHELX, *Acta Crystallogr. Sect. A Found. Crystallogr.*, 2008, **64**, 112–122.

4 M. J. Frisch, G. W. Trucks, H. B. Schlegel, G. E. Scuseria, M. a. Robb, J. R. Cheeseman, G. Scalmani, V. Barone, G. a. Petersson, H. Nakatsuji, X. Li, M. Caricato, a. V. Marenich, J. Bloino, B. G. Janesko, R. Gomperts, B. Mennucci, H. P. Hratchian, J. V. Ortiz, a. F. Izmaylov, J. L. Sonnenberg, Williams, F. Ding, F. Lipparini, F. Egidi, J.

Goings, B. Peng, A. Petrone, T. Henderson, D. Ranasinghe, V. G. Zakrzewski, J. Gao, N. Rega, G. Zheng, W. Liang, M. Hada, M. Ehara, K. Toyota, R. Fukuda, J. Hasegawa, M. Ishida, T. Nakajima, Y. Honda, O. Kitao, H. Nakai, T. Vreven, K. Throssell, J. a. Montgomery Jr., J. E. Peralta, F. Ogliaro, M. J. Bearpark, J. J. Heyd, E. N. Brothers, K. N. Kudin, V. N. Staroverov, T. a. Keith, R. Kobayashi, J. Normand, K. Raghavachari, a. P. Rendell, J. C. Burant, S. S. Iyengar, J. Tomasi, M. Cossi, J. M. Millam, M. Klene, C. Adamo, R. Cammi, J. W. Ochterski, R. L. Martin, K. Morokuma, O. Farkas, J. B. Foresman and D. J. Fox, 2016, Gaussian 16, Revision C.01, Gaussian, Inc., Wallin.

5 C. Naim, F. Castet and E. Matito, Impact of van der Waals interactions on the structural and nonlinear optical properties of azobenzene switches, *Phys. Chem. Chem. Phys.*, 2021, **23**, 21227–21239.

6 S. Grimme, J. Antony, S. Ehrlich and H. Krieg, A consistent and accurate ab initio parametrization of density functional dispersion correction (DFT-D) for the 94 elements H-Pu, *J. Chem. Phys.*, , DOI:10.1063/1.3382344.

7 F. H. Allen, O. Kennard, D. G. Watson, L. Brammer, A. G. Orpen and R. Taylor, Tables of bond lengths determined by x-ray and neutron diffraction. Part 1. Bond lengths in organic compounds, *J. Chem. Soc. Perkin Trans. 2*, 1987, 1–19.

8 P. R. Spackman, M. J. Turner, J. J. McKinnon, S. K. Wolff, D. J. Grimwood, D. Jayatilaka and M. A. Spackman, CrystalExplorer: A program for Hirshfeld surface analysis, visualization and quantitative analysis of molecular crystals, *J. Appl. Crystallogr.*, 2021, **54**, 1006–1011.

9 C. F. Mackenzie, P. R. Spackman, D. Jayatilaka and M. A. Spackman, CrystalExplorer model energies and energy frameworks: Extension to metal coordination compounds, organic salts, solvates and open-shell systems, *IUCrJ*, 2017, **4**, 575–587.

10 S. P. Thomas, P. R. Spackman, D. Jayatilaka and M. A. Spackman, Accurate Lattice Energies for Molecular Crystals from Experimental Crystal Structures, *J. Chem. Theory Comput.*, 2018, **14**, 1614–1623.